Pinned or moving: States of a single shock in a ring

Parna Roy,[1,*] Anjan Kumar Chandra,[2,†] and Abhik Basu[1,‡]
[1]*Condensed Matter Physics Division, Saha Institute of Nuclear Physics, Calcutta 700064, West Bengal, India*
[2]*Malda College, Malda 732101, West Bengal, India*

(Received 21 May 2019; accepted 26 May 2020; published 1 July 2020)

Totally asymmetric exclusion processes (TASEPs) with open boundaries are known to exhibit moving shocks or delocalized domain walls (DDWs) for sufficiently small equal injection and extraction rates. In contrast, TASEPs in a ring with a single inhomogeneity display pinned shocks or localized domain walls (LDWs) under equivalent conditions [see, e.g., H. Hinsch and E. Frey, Phys. Rev. Lett. **97**, 095701 (2006)]. By studying periodic exclusion processes composed of a driven (TASEP) and a diffusive segment, we discuss gradual fluctuation-induced depinning of the LDW, leading to its delocalization and formation of a DDW-like domain wall, similar to the DDWs in open TASEPs *in some limiting cases* under long-time averaging. This smooth crossover is controlled essentially by the fluctuations in the diffusive segment. Our studies provide an explicit route to control the quantitative extent of domain-wall fluctuations in driven periodic inhomogeneous systems, and should be relevant in any quasi-one-dimensional transport processes where the availability of carriers is the rate-limiting constraint.

DOI: 10.1103/PhysRevE.102.012105

I. INTRODUCTION

Correlated fluctuations in statistical mechanics is of great importance, and can be decisive in controlling the macroscopic behavior of systems in many circumstances, especially in low dimensions. For instance, long-ranged fluctuations near the critical point in the equilibrium Ising model at three dimensions can change the universal scaling of the thermodynamic and correlation functions predicted by the mean-field theories that ignores the fluctuations [1]. Fluctuations can altogether destroy the phase transitions at sufficiently low dimensions, e.g., the one-dimensional (1D) equilibrium Ising model [1]. Fluctuations can be important in nonequilibrium systems as well, e.g., in the Kardar-Parisi-Zhang (KPZ) equation for surface growth phenomena [2], where fluctuations coupled with nonlinear effects can lead to a nontrivial phase transition between a (low noise) smooth phase and a (high noise) rough phase at dimensions greater than two. It is thus imperative to study the effects of fluctuations in physical systems. Since out-of-equilibrium systems do not yet have a general theoretical framework, it is useful to study simple nonequilibrium models in this context.

The totally asymmetric simple exclusion process (TASEP) with open boundaries was originally proposed as a simple model for the motion of molecular motors in eukaryotic cells [3]. Subsequently, it was reinvented as a paradigmatic one-dimensional (1D) model for nonequilibrium statistical mechanics, that shows boundary-induced phase transitions characterized by α and β, the entry and exit rates [4]. Extensive Monte Carlo simulations (MCSs) supplemented by mean-field theories (MFTs) reveal that for $\alpha = \beta < 1/2$ with unit hopping rate in the bulk for the unidirectional movement, the steady-state density profiles show a *moving shock* or *delocalized domain wall* (DDW) that moves randomly and unrestrictedly along the whole TASEP [5]. This is usually explained in terms of completely uncorrelated entry and exit events.

Studies on various aspects of TASEP and its application have a long history. For instance, the exact steady states of TASEP in some cases have been expressed as a matrix product form [6]. The notable biologically relevant applications of TASEP include biological transport [7], motor proteins [8], intracellular transport involving both diffusive and active motion [9], and cellular automata-based modeling studies [10]. TASEP is also relevant for studies on fast ionic conductors [11] and traffic movement [12].

There are several related theoretical studies as well, e.g., Ref. [13] has studied driven Brownian motion of hard rods in a given potential and Ref. [14] has studied dynamic processes for a driven diffusive two-lane system. TASEP has been considered in a periodic lattice as well. This could be of relevance, e.g., in the traffic of molecular motors in closed compartments [15], where spatially varying steady-state densities and "traffic jams" of motors have been found, and colloidal motion along periodic potentials with temporal oscillations [16], where directed motion could be induced under certain circumstances. In periodic TASEP (i.e., TASEP on a ring) macroscopically nonuniform steady-state densities can emerge when translational invariance is explicitly broken. This can happen in a variety of ways. For instance, TASEP on a ring with a single bottleneck or a defect site with a lower hopping rate than the remaining system can show a pinned shock or LDW for moderate average densities [17,18]. In

*parna.roy14@gmail.com
†anjanphys@gmail.com
‡abhik.123@gmail.com

yet another manifestation of the breakdown of translational invariance, a closed system composed of two segments of equal size—a TASEP and a diffusive lane with exclusion, executing what is known as the *symmetric exclusion process* or SEP—also shows an LDW in the steady states for moderate average densities [19]. Overall, periodic TASEPs with one inhomogeneity generically display a single LDW for moderate densities. In contrast, inhomogeneous TASEP on a ring can display two or more DDWs only when there is more than one bottleneck of equal strength [17,20].

Focusing particularly on the model in Ref. [19], we note that by varying the model parameters the model can be in the low density (LD), high density (HD), and maximal current (MC) phases, in direct analogy with an open TASEP. This model also displays a "domain-wall phase" or a coexistence region, where a single LDW is observed, revealed by both MCS and MFT studies. That an LDW and not a DDW is observed is attributed to the overall particle number conservation and the associated correlated particle entry and exit in the TASEP segment of the ring. Nonetheless, it still begs the question why it should be so, given that in a periodic system, the TASEP segment by itself does not conserve the particle number (although the degree of nonconservation should depend on the size of the non-TASEP segment), and hence, at least partly resembles an open TASEP. This in turn opens the possibility that it may be possible to observe a single domain wall that may naively resemble a DDW, in contrast to what has actually been found so far in the studies of Ref. [19]. While larger particle number fluctuations in TASEP are generally expected to enhance the fluctuations of the LDW, systematic results on this phenomenon are lacking. It is thus pertinent to ask: Can a single LDW observed in periodic TASEPs with a single inhomogeneity be converted into a *single* DDW-like domain wall, resembling DDWs in open TASEPs? If so, under what situations and how—is it a *smooth* or a *sudden* transition? In particular, how should the model parameters scale in order for the systems to display this phenomenon? This forms the basic questions addressed in this work.

We argue in this work that the particle number fluctuations in the TASEP segment that controls the LDW fluctuations, can be controlled by the particle content in the non-TASEP-diffusive segment via particle number conservation. To test this proposition, we construct several different but related conceptual models, each having one TASEP and one diffusive segment. The diffusive part breaks the translational invariance and plays the role of an extended inhomogeneity [19]. Each of these models show an LDW in the TASEP segment for small average particle content in the diffusive segment in the steady states; as the latter rises, the LDW gradually delocalizes to a DDW-like domain wall that spans the whole length of the TASEP segment. This visually resembles a standard TASEP and is indistinguishable from a DDW in an open TASEP. This shows robustness of the mechanism of delocalization. Furthermore, we are able to obtain the necessary relations between model parameters that define the relative size of the segments and the number density of particles for observing a single LDW, whose fluctuations diverge with the size of the TASEP segment. These results are generic and should apply in any quasi-1D transport processes with directed single-file motion where a finite supply of particles is the limiting constraint, e.g., motors in cells, cyclic translocation of ribosomes along mRNA loops, and vehicular transport networks in closed geometries. These results can also be tested in carefully designed *in vitro* experiments on the collective motion of driven particles along a closed track that enforces directional motion only along a segment of the system. Since an LDW implies a phase-separated state in a closed system, whereas a DDW may be viewed as "mixing" of the two states (under long-time averages), the emergence of a DDW-like domain wall due to enhanced fluctuations could be interpreted as destruction of phase separation due to large fluctuations. Thus from a theoretical standpoint, this is like a nonequilibrium analog of the destruction of the ordered phases in low-dimensional equilibrium systems by thermal noises.

The remaining part of this article is structured as follows: In Sec. II we construct our models. In Secs. III A and III B the nature of the domain walls in the models are discussed. We summarize our results in Sec. IV. Some calculational details including the phase diagrams are given in the Appendices at the end.

II. MODELS FOR PERIODIC EXCLUSION PROCESSES

We study two related conceptual models defined on a ring, each of which consists of a diffusive part $\mathcal{S}$ and a driven part $\mathcal{T}$ joined at junctions A and B. In $\mathcal{T}$, particle hopping is unidirectional at a unit rate that is subject to exclusion, whereas in $\mathcal{S}$ particles jump independently and randomly to the neighboring site at rate D with equal probability to the left and right. Particle dynamics in $\mathcal{S}$ may or may not be subject to exclusion. We consider both the possibilities for $\mathcal{S}$.

The segment $\mathcal{T}$ executing asymmetric exclusion processes has N sites, whereas the diffusive segment $\mathcal{S}$ that has $\tilde{N} = rN$ sites with r can be smaller or larger than unity. In order to define the models formally, we denote the location of the lattice sites and occupation numbers by $i \in [1, N]$ and n_i for $\mathcal{T}$ and $\tilde{i} \in [1, rN]$ and $\tilde{n}_i$ for $\mathcal{S}$, respectively. The total number of particles

$$N_p = \sum_{i=1}^{N} n_i + \sum_{\tilde{i}=1}^{rN} \tilde{n}_i \tag{1}$$

is conserved.

The segment $\mathcal{T}$ is identical in both the models. These two models are, however, distinguished by their respective diffusive segments $\mathcal{S}$. The details are as follows:

(i) In model I, unlike in $\mathcal{T}$, we do not impose any condition of exclusion in $\mathcal{S}$, i.e., a site in $\mathcal{S}$ is here allowed to accommodate any number of particles without restrictions (see Fig. 1 for a schematic diagram).

As a result, the overall particle density

$$n_p = \frac{N_p}{N(1+r)} \tag{2}$$

is *not* restricted to [0,1]. Furthermore, particles can exit $\mathcal{T}$ at a given rate β to enter into $\mathcal{S}$ that is completely unaffected by the occupation of the site $\tilde{i} = 1$ in $\mathcal{S}$. Thus, β is a tuning parameter for model I. Hence, the steady states of model I are parametrized by three parameters: D, n_p, and β.

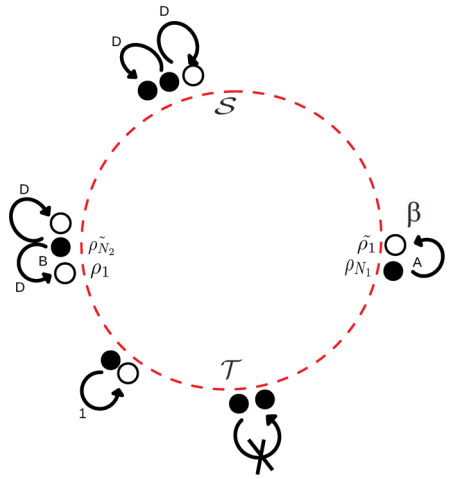

FIG. 1. Schematic diagram for model I. Particles in segment $\mathcal{S}$ diffuse, whereas in $\mathcal{T}$ they undergo asymmetric exclusion processes. Segments $\mathcal{T}$ and $\mathcal{S}$ are joined at junctions A and B. Sites in $\mathcal{S}$ can accommodate any number of particles. Filled circles represent occupied sites; empty circles represent vacant sites.

(ii) In contrast, in model II, we impose exclusion in $\mathcal{S}$. Thus the dynamics in the whole ring in model II is subject to exclusion; each site in $\mathcal{T}$ or $\mathcal{S}$ can be occupied by at most one particle (see Fig. 2 for a schematic diagram).

Hence, the particle density $n_p = \frac{N_p}{N(1+r)} \in [0, 1]$ necessarily, since there could be at most one particle per site. Notice that the rate at which particles can exit $\mathcal{T}$ and move to $\mathcal{S}$*does depend* on the occupation at $\tilde{i} = 1$—a direct consequence of exclusion in $\mathcal{S}$. Thus model II is a two-parameter model: n_p and D.

Model II directly generalizes the model studied in Ref. [19]; several other generalizations of the model in Ref. [19] have been proposed. For instance, effects of biased diffusion on the phase diagram [21], two-lane diffusive lanes

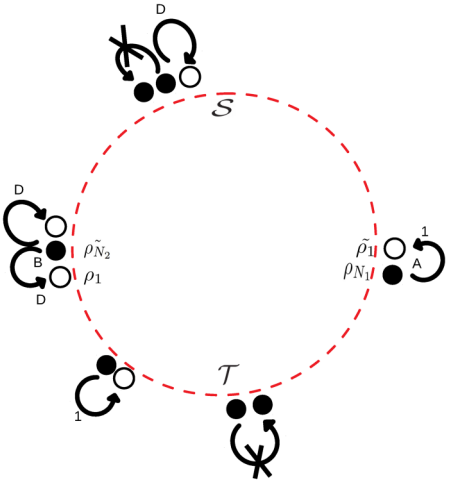

FIG. 2. Schematic diagram of model II. Particles in segment $\mathcal{S}$ diffuse subject to exclusion, whereas in $\mathcal{T}$ they undergo asymmetric exclusion processes. Segments $\mathcal{T}$ and $\mathcal{S}$ are joined at junctions A and B. Filled circles represent occupied sites; empty circles represent vacant sites.

with a current splitting parameter [22], asymmetrically coupled three-lane system [23], and the competition between the topology of the network and Langmuir kinetics [24] have been studied. In contrast, the dynamics of model I has no simple direct relation with the model of Ref. [19]. Models I and II are thus identical in their TASEP segments $\mathcal{T}$, but differ in not having or having exclusion imposed on the respective diffusive segments $\mathcal{S}$, as elucidated in the model diagrams (1) and (2), respectively. These differences are significant: model I is a three-parameter model, whereas model II is a two-parameter model. Any general results from two seemingly different models will underscore an underlying common physical mechanism independent of model details. In fact, we find that all the models are shown to display similar deconfinement of LDWs as the *total particle content* of $\mathcal{S}$ rises, a feature that is attributed to enhanced fluctuations in $\mathcal{S}$ (see below).

III. STEADY-STATE DENSITY PROFILES

We use MFT together with extensive (MCS of the models to obtain the steady-state density profiles. In MFT approaches, the system is considered as a collection of one TASEP ($\mathcal{T}$) with open boundaries having effective entry and exit rates and a diffusive lane ($\mathcal{S}$) again with open boundaries, having its own effective entry and exit rates [19]. These effective rates are determined from the condition of particle current conservation in the steady states. We then use them in conjunction with the known results for the TASEP and diffusive lane with open boundaries to obtain the density profiles here.

We denote the steady-state density at a particular site m in $\mathcal{T}$ as $\rho_m = \langle n_m \rangle$ and in $\mathcal{S}$ as $\tilde{\rho}_m = \langle \tilde{n}_m \rangle$, where $\langle \cdots \rangle$ represent time averages in the steady states. MF analysis entails taking the continuum limit with $\rho(x)$ and $\tilde{\rho}(\tilde{x})$ as the densities in $\mathcal{T}$ and $\mathcal{S}$, where $x = i/N$ and $\tilde{x} = \tilde{i}/N$. In the thermodynamic limit, $N \gg 1$ and consequently x and $\tilde{x}$ vary effectively continuously with $0 \leqslant x \leqslant 1$, $0 \leqslant \tilde{x} \leqslant r$. We further introduce the following notations for the stationary densities at junctions B and A, respectively: $\rho(x = 0) = \alpha$ and $\rho(x = 1) = (1 - \beta)$ for $\mathcal{T}$ according to the standard TASEP convention and $\tilde{\rho}(\tilde{x} = 0) = \gamma$ and $\tilde{\rho}(\tilde{x} = r) = \delta$ for $\mathcal{S}$. The MFT analysis is complemented by extensive MCS studies using random sequential updates.

A. Domain walls in model I

In model I, multiple occupancy in each site of $\mathcal{S}$ is allowed. In steady states, $\tilde{\rho}(\tilde{x})$ is given by a linear profile in MFT:

$$\tilde{\rho}(\tilde{x}) = \gamma - (\gamma - \delta)\tilde{x}/r. \tag{3}$$

The corresponding current in $\mathcal{S}$ is given by

$$J_{\mathcal{S}} = (\gamma - \delta)D/Nr. \tag{4}$$

This must be equal to $J_{\mathcal{T}} \sim O(1)$ in steady states. Now $J_{\mathcal{S}}$, as given in (4), can be $O(1)$, e.g., when (i) $\gamma \sim \mathcal{O}(N)$, so that the difference $\gamma - \delta \sim O(N)$ together with $D \sim O(1)$. We call this model IA or (ii) $D \sim O(N)$, but $\gamma, \delta \sim O(1)$. We call this model IB [25].

It is instructive to first consider the phases and the ensuing phase diagrams of models IA and IB in qualitative terms.

Comparing with an open TASEP, LD and HD phases are to be found for $\alpha < \beta$, $\alpha < 1/2$ and $\beta < \alpha$, $\beta < 1/2$, respectively, whereas, for $\alpha, \beta \geqslant 1/2$ MC phase ensues. Unlike in an an open TASEP, where both α and β are free parameters that can be tuned, in model IA or IB, α is to be determined from the various conditions available (see below), while β remains free. Consider the phases for $\beta < 1/2$ in model IA. By tuning n_p and D, α may be varied, as shown below. Thus in the n_p-D plane, regions with $\alpha < \beta < 1/2$ correspond to the LD phase; the remaining regions where $\alpha > \beta < 1/2$ correspond to the HD phase. However, there is no MC phase for $\beta < 1/2$. Further, regions corresponding to $\alpha = \beta < 1/2$, which for an open TASEP correspond to a DDW that spans the entire TASEP, should imply domain walls, the investigation of whose nature is a primary goal of this work. In contrast when $\beta > 1/2$, in the n_p-D plane one obtains the LD phase in the region with $\alpha < 1/2$. In the remaining region for which $\alpha > 1/2$, $\beta > 1/2$, the MC phase is found. Thus, there are LD and MC phase with no HD phase. This physical picture remains unchanged in Model IB. In the main text, we focus on the nature of the domain walls and set $\beta < 1/2$. The detailed phase diagrams for models IA and IB obtained from MFT and MCS studies are given in the Appendices.

To proceed further, we assume a domain wall with a mean position x_w. Thus the steady-state density in $\mathcal{T}$ is

$$\rho(x) = \beta + \Theta(x - x_w)(1 - 2\beta), \tag{5}$$

where we have used $\alpha = \beta$; here $\Theta(x)$ is the Heaviside Θ function at x. The corresponding steady-state current in $\mathcal{T}$ is given by

$$J_{\mathcal{T}} = \alpha(1 - \alpha) = \beta(1 - \beta). \tag{6}$$

The incoming current to site $x = 0$ at $\mathcal{T}$ is $\delta D(1 - \alpha)$. By using the current conservation in the steady state, we obtain

$$\delta D(1 - \alpha) = \beta(1 - \beta). \tag{7}$$

As long as there is a particle in the last site $i = N$ of $\mathcal{T}$, it jumps to the first site $\tilde{x} = 0$ of $\mathcal{S}$ with probability β, independent of how many particles are already there in $\tilde{x} = 0$, i.e., independent of γ. Since multiple occupancy is allowed in $\mathcal{S}$, the mean particle number $\overline{N}_s$ in $\mathcal{S}$ in the steady states can be both larger or smaller than $\tilde{N} = Nr$.

1. Domain walls in model IA

Consider a domain wall in model IA. Here, $D \sim O(1)$. Domain-wall position x_w can be calculated from the conservation of total particle number. This requires solving for $\tilde{\rho}(\tilde{x})$, which in turn requires knowledge of γ and δ in terms of the model parameters. This can be done by using the conservation of the current in the system in the steady state, i.e., by equating $J_{\mathcal{S}}$ in (4) with $J_{\mathcal{T}}$ given by (6). Straightforward algebra, whose details interested readers can find in Appendix A, gives for x_w,

$$x_w(2\beta - 1) + (1 - \beta) + \frac{Nr^2}{2D}\left[\beta(1 - \beta) + \frac{\beta}{Nr}\right] + \frac{\beta r}{2D} = n_p(1 + r). \tag{8}$$

Equation (8) clearly yields x_w *uniquely* in terms of β, n_p, r, D. Since $0 < x_w < 1$, n_p must be small enough to make Eq. (8) valid. Since the DW position x_w is fixed, this implies an LDW within our MFT. In Fig. 3 we have plotted the stationary density for $N = 400$, $r = 1$, and $n_p = 0.6$ from both MFT and MCS, both of which clearly show an LDW, in good agreement with each other. The picture is dramatically different in Fig. 4, where we have plotted the stationary density in $\mathcal{T}$ for $N = 1000$, $r = 2$, and $n_p = 50.5$, from the MCS study. The MCS study unexpectedly shows a domain wall that resembles a DDW in an open TASEP, whereas MFT results continue to predict an LDW, along with its precise location. This delocalized nature of the domain wall in the MCS study can also be seen in the corresponding kymograph (Fig. 15) in Appendix A that clearly shows that the spatial extent of the domain-wall movements due to its fluctuations spans the entire length of $\mathcal{T}$. Notice that between Fig. 3 and Fig. 4, all that changes is the particle number in $\mathcal{S}$, relative to the same in $\mathcal{T}$. Thus, an enhanced particle number in $\mathcal{S}$ can delocalize an LDW in $\mathcal{T}$, as mentioned in the beginning of this article. Before we analyze and explain this behavior, we first consider the nature of domain walls in model IB below.

2. Domain walls in model IB

Let us now study model IB, for which D scales with the system size N; we set $D = dN$ with $d \sim O(1)$. For a domain wall at x_w, following the logic outlined for model IA above and using the overall particle number conservation, we obtain (see Appendix B)

$$x_w(2\beta - 1) + (1 - \beta) + \frac{r^2}{2d}[\beta(1 - \beta)] = n_p(1 + r). \tag{9}$$

Since β is a fixed model parameter, x_w is uniquely determined, implying an LDW. In Fig. 5, we have plotted $\rho(x)$ versus x for $N = 400$, $r = 1$, and $n_p = 0.4$ for different β and $d = 0.4$, from both MCS and MFT studies. Unsurprisingly, we find an LDW; MFT and MCS results agree with each other well.

Consider now Fig. 6, where we have plotted $\rho(x)$ versus x for $N = 1000$, $r = 2$, and $n_p = 10.0$ for different d and $\beta = 0.1$. Unexpectedly, we obtain a single DDW-like delocalized LDW from the MCS study, whereas the MFT still predicts a conventional localized LDW. That $\rho(x)$ in Fig. 6 indeed shows a delocalized LDW can be confirmed from the corresponding kymograph in Fig. 17 in Appendix B which clearly shows that the fluctuation of the domain spans the entire length of $\mathcal{T}$, confirming a delocalized LDW. Similar to the change in the nature of the LDW in model IA with a rise in the particle number in $\mathcal{S}$, as revealed by Figs. 3 and 4 above, here too all that changes between Figs. 5 and 6 is the total particle content in $\mathcal{S}$, relative to the same in $\mathcal{T}$. Therefore, the existence of a single DDW-like system-spanning LDW, being independent of the precise dynamics in $\mathcal{S}$, is fairly robust.

3. Pinned or moving shocks?

This conundrum between an LDW and a DDW-like domain wall can be resolved when fluctuations are taken into account. Strict particle number conservation in models IA and IB always ensures unique determination of x_w that must imply a conventional LDW. In contrast, in an open TASEP, total

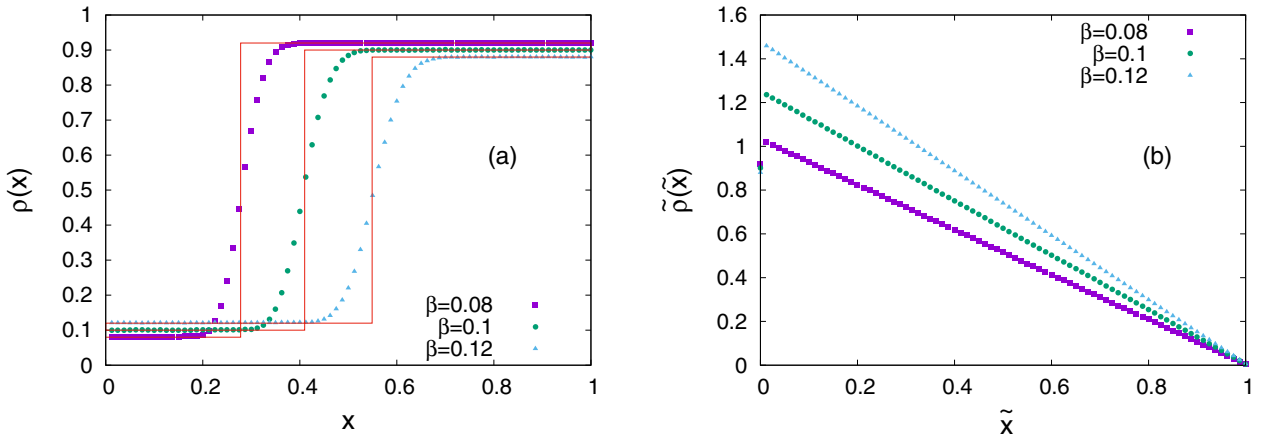

FIG. 3. Plots of (a) $\rho(x)$ versus x, and (b) $\tilde{\rho}(\tilde{x})$ versus $\tilde{x}$ for model IA for $N = 400$, $r = 1$, $n_p = 0.6$, and $D = 28.8$ for three different values of β. Step functions in red; continuous lines are the MFT predictions for $\rho(x)$; dotted lines correspond to $\rho(x)$ (left) and $\tilde{\rho}(\tilde{x})$ from MCS studies. These show LDWs in $\mathcal{T}$.

particle number in the steady state is conserved only on "average"; as a result, MFT does not give any unique mean position for the domain wall.

In the present study, for any x_w between 0 and 1, $J_{\mathcal{T}}$ is the same; the domain-wall position can move anywhere in the system, keeping the current in the TASEP unchanged. Such a movement is necessarily associated with the fluctuations in the total number of particles in $\mathcal{T}$. For the domain-wall position fluctuations covering the entire length N of an open TASEP, the size of the associated number fluctuations is $O(N)$. Thence, in order for a single DDW-like domain wall to exist in $\mathcal{T}$, fluctuations of x_w is to occur over a scale comparable to N, which in turn means particle fluctuations of size $O(N)$ in $\mathcal{T}$. Since the total number of particles is constant, fluctuations in $\mathcal{T}$ are bounded by fluctuations in the mean particle number $\overline{N}_s$ in $\mathcal{S}$ with $\overline{N}_s$ given by

$$\overline{N}_s = \int_0^r \tilde{\rho}(x)d\tilde{x} = \int_0^r [\delta + (\gamma - \delta)\tilde{x}/r]d\tilde{x}. \tag{10}$$

With values of γ and δ already obtained in the MFT above, $\overline{N}_s$ can be obtained for models IA and IB. For example, in model IA, $\overline{N}_s$ is given by

$$\overline{N}_s = N\left\{\frac{Nr^2}{2D}\left[\alpha(1-\alpha) + \frac{\alpha}{Nr}\right] + \frac{r\alpha}{2D}\right\}. \tag{11}$$

In model IB, $D \to \infty$ in the thermodynamic limit. The total particles in $\mathcal{S}$, $\overline{N}_s$, is given by

$$\overline{N}_s = N\left[\frac{Nr^2}{2D}\alpha(1-\alpha)\right] = N\left[\frac{r^2}{2d}\alpha(1-\alpha)\right]. \tag{12}$$

Thus, for large N and large r, $\overline{N}_s \sim N^2r^2$ in model IA, and $\overline{N}_s \sim Nr^2$ in model IB. As mentioned above, for a DDW-like domain wall to exist in $\mathcal{T}$ of a span of size $O(N)$, the typical particle number fluctuations in $\mathcal{T}$ are $\sim O(N)$. In order to maintain overall particle number conservation, $\mathcal{S}$ must also have particle number fluctuations of size $\sim O(\overline{N})$. In order to quantify this, we calculate the variances Δ_T and Δ_S of particle numbers $N_{\mathcal{T}}$ and $N_{\mathcal{S}}$ in $\mathcal{T}$ and $\mathcal{S}$, respectively, in the steady states. We define

$$\Delta_T = \langle N_{\mathcal{T}}^2\rangle - (\overline{N}_{\mathcal{T}})^2, \quad \Delta_S = \langle N_{\mathcal{S}}^2\rangle - (\overline{N}_{\mathcal{S}})^2, \tag{13}$$

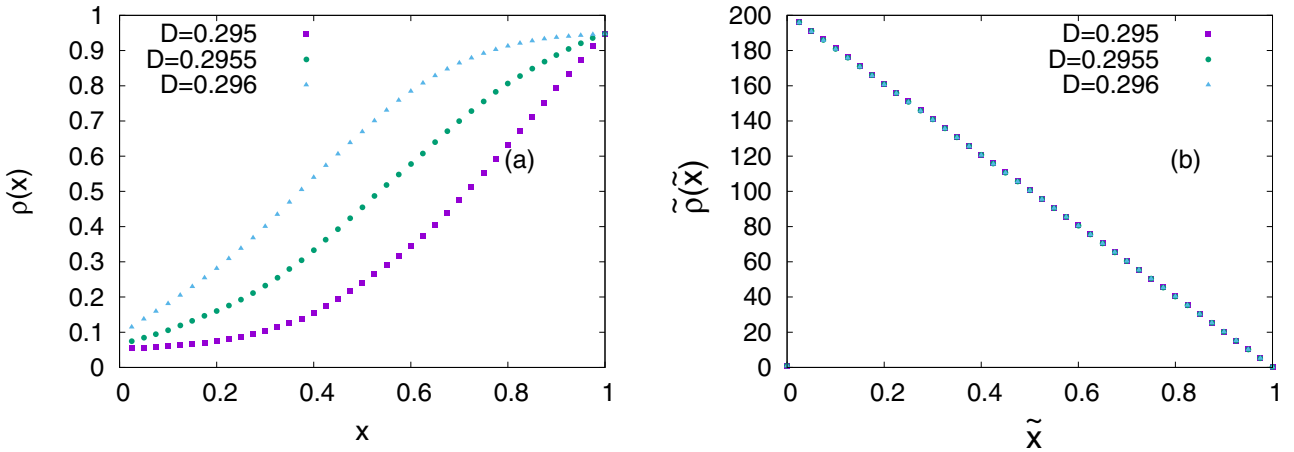

FIG. 4. Plots of (a) $\rho(x)$ versus x, and (b) $\tilde{\rho}(\tilde{x})$ versus $\tilde{x}$ for model IA for $N = 1000$, $r = 2$, and $n_p = 50.5$ for different values of D and $\beta = 0.0522$. MCS studies show a DDW-like domain wall, whereas MFT predicts conventional LDWs (not shown).

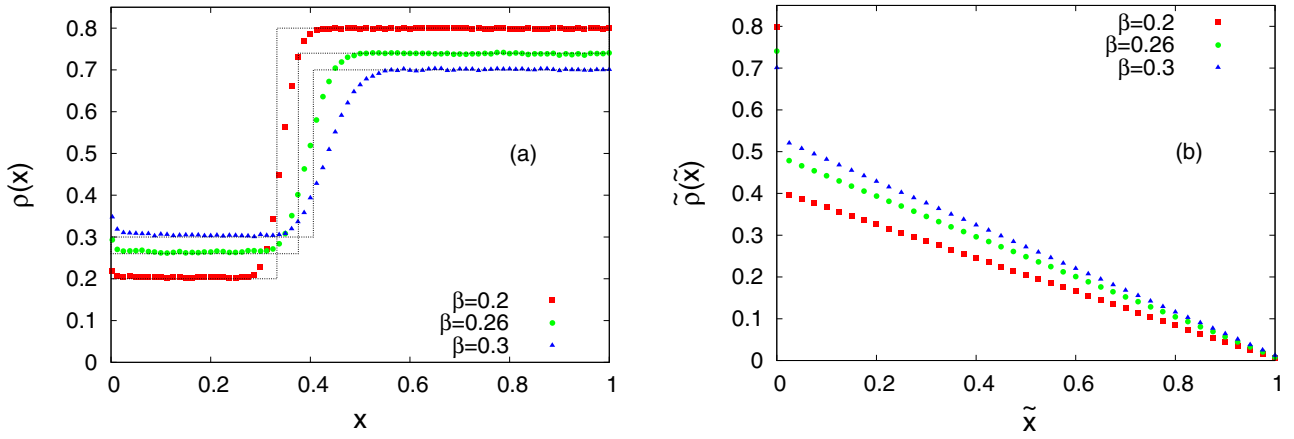

FIG. 5. Plot of (a) $\rho(x)$ versus x, and (b) $\tilde{\rho}(\tilde{x})$ versus $\tilde{x}$ for model IB with $N = 400$, $r = 1$, $n_p = 0.4$, and $d = 0.4$ for different values of β, from both MCS and MFT studies. Step functions in black; continuous lines in the left figure represent MFT predictions for $\rho(x)$; dotted lines in both figures are from the MCS studies. Both studies reveal LDWs for $\rho(x)$.

where $N_{\mathcal{T}}$ is the instantaneous particle number in $\mathcal{T}$ and $\overline{N}_{\mathcal{T}}$ is its average; $N_{\mathcal{S}}$ is the instantaneous particle number in $\mathcal{S}$ and $\overline{N}_{\mathcal{S}}$ is its average; $\langle \cdots \rangle$ implies averages in the steady states. That $\Delta_{\mathcal{T}}$ rises monotonically with $\Delta_{\mathcal{S}}$ in the steady states of both model IA and model IB is readily seen in Fig. 7. In fact, within our numerical accuracy, these two are found to be equal, in agreement with our arguments above.

We now estimate $\Delta_{\mathcal{S}}$ heuristically. The size of typical fluctuations in $\mathcal{T}$ is $\sim\sqrt{\Delta_{\mathcal{T}}}$. In analogy with an ideal gas or with a collection of noninteracting particles, we expect variance $\Delta_{\mathcal{S}} \sim \overline{N}_s$. Now $\overline{N}_s$ can be raised by increasing n_p or r. For a DDW that spans the entire $\mathcal{T}$, $\sqrt{\Delta_{\mathcal{T}}} \sim \sqrt{\Delta_{\mathcal{S}}} \sim \sqrt{\overline{N}_s} \sim O(N)$, so that the fluctuations in x_w relative to N (the size of $\mathcal{T}$) do *not* vanish for $N \to \infty$. Clearly, in the limit of $n_p, r \ll 1$, $\Delta_{\mathcal{S}}$ should be very small (since there are too few particles in $\mathcal{S}$); fluctuations in x_w relative to N are negligible; hence an LDW is observed. In contrast, for $n_p, r \gg 1$, $\Delta_{\mathcal{S}}$ is expected to be large; hence fluctuations in x_w become comparable to N, making the LDW visually appearing like a DDW in an open TASEP. More formally, ignoring the spatial extent of $\mathcal{S}$, and instead treating it as a bath having $\overline{N}_{\mathcal{S}}$ number of particles on average, we assume each particle, deemed identical, can leave $\mathcal{S}$ or return to it (due to the exchanges between $\mathcal{S}$ and $\mathcal{T}$), controlled by an identical probability distribution with a variance σ. We then estimate

$$\Delta_{\mathcal{S}} \sim \sum_{m=1}^{\overline{N}_{\mathcal{S}}} \sigma^2 \sim \overline{N}_{\mathcal{S}} \sigma^2, \tag{14}$$

giving $\Delta_{\mathcal{S}} \sim \overline{N}_{\mathcal{S}}$. As argued above, typical particle fluctuations in $\mathcal{T}$ are $\sim\sqrt{\Delta_{\mathcal{T}}} \sim O(N)$ for a domain wall that resembles a DDW in an open TASEP. Further, $\Delta_{\mathcal{T}} \sim \Delta_{\mathcal{S}}$ in the steady state, giving $\sqrt{\Delta_{\mathcal{S}}} \sim \sqrt{\overline{N}_{\mathcal{S}}} \sim O(N)$ as the threshold for a DDW-like domain wall in $\mathcal{T}$. From (A4), for large N

$$n_p r \sim N r^2 \tag{15}$$

for model IA. Further, from (11)

$$\overline{N}_{\mathcal{S}} \sim N^2 r^2 \sim N n_p r \tag{16}$$

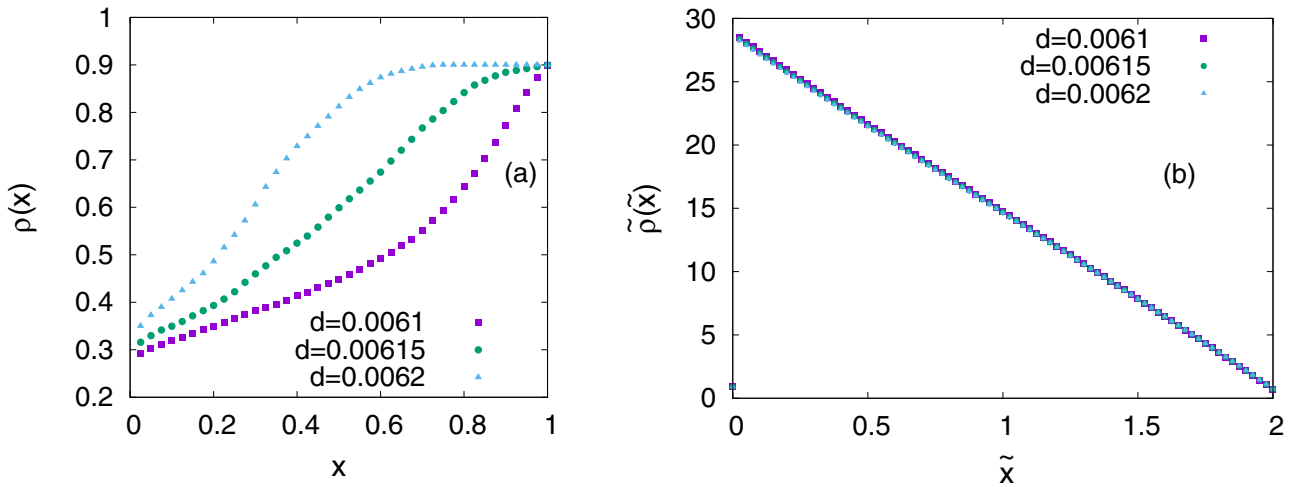

FIG. 6. Plots of (a) $\rho(x)$ versus x and (b) $\tilde{\rho}(\tilde{x})$ versus $\tilde{x}$ for model IB with $N = 1000$, $r = 2$, and $n_p = 10.0$ for different d and $\beta = 0.1$. MCS studies exhibit DDW-like domain walls in $\mathcal{T}$; in contrast, MFT yields LDWs (not shown).

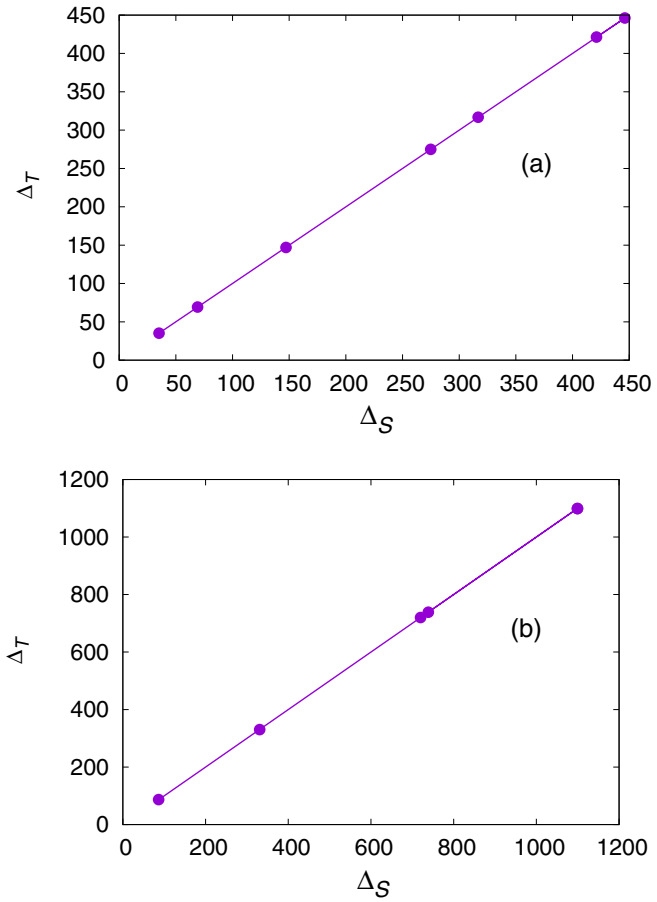

FIG. 7. Plot of Δ_S versus Δ_T for (a) model IA and (b) model IB.

in the large N limit for model IA. Using the condition for a DDW-like domain wall in model IA, we then find

$$\sqrt{\overline{N}_{\mathcal{S}}} \sim \sqrt{Nn_p r} \sim O(N) \Rightarrow n_p r \sim O(N) \tag{17}$$

as the necessary condition for an LDW taking the shape of a DDW-like domain wall that spans the whole of $\mathcal{T}$ in model I. Similarly, by using (B4) we obtain

$$n_p r \sim r^2 \tag{18}$$

for model IB. Further, using (12) and noting that $D \propto N$ in model IB,

$$\overline{N}_{\mathcal{S}} \sim Nr^2 \sim Nn_p r \tag{19}$$

in the large N limit for model IB. Now following the logic outlined for model IA above, we get

$$n_p r \sim O(N) \tag{20}$$

as the threshold for a DDW-like domain wall in model IB that spans the whole of $\mathcal{T}$ due to the particle number fluctuations. Surprisingly, the product $n_p r$ must scale with N in both model IA and model IB for a DDW; the prefactors omitted in (17) and (20) are $O(1)$ constants which depend on the specific model under consideration (IA or IB). Our MCS results on DDW are consistent with this. Notice that the boundary line (17) or (20) in the n_p-r plane, is *not sharp*, since the transition

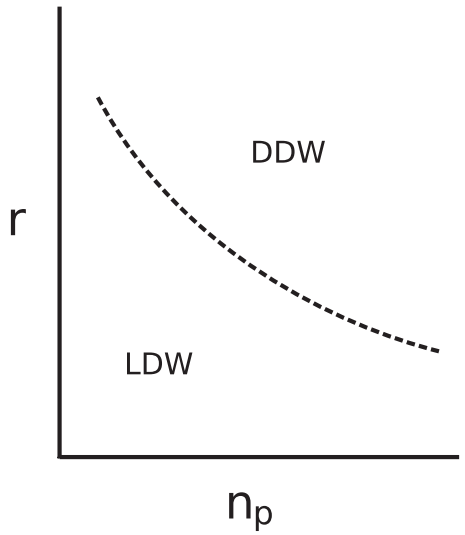

FIG. 8. A schematic state diagram for model IA or IB in the n_p-r plane for a fixed N (assumed large) when the conditions of a domain wall are fulfilled. The broken demarcation line is not a sharp boundary (see text).

from an LDW to a DDW is gradual. A schematic state diagram of model IA or IB in the n_p-r plane for a fixed N (assumed large) when the conditions of a domain wall are fulfilled, showing the regions corresponding to a conventional LDW and an LDW that takes the form of a DDW in an open TASEP, is given in Fig. 8.

B. Steady density profiles in model II

Unlike models IA and IB, sites in $\mathcal{S}$ of model II can accommodate a maximum one particle per site, i.e., exclusion is imposed on $\mathcal{S}$ as well. Nonetheless, the current $J_{\mathcal{S}}$ is still given by (4). Due to exclusion, densities γ and δ cannot exceed 1. In the steady state, when $J_{\mathcal{S}} = J_{\mathcal{T}}$, in order to have a finite current in the thermodynamic limit, we must make $D \propto N$. As in model IB, we define $D = Nd$, so that the current in $\mathcal{S}$ is written as

$$J_{\mathcal{S}} = (\gamma - \delta)d/r, \tag{21}$$

as in model IB. In steady states, the particle current is constant throughout the system. Considering this at the two junctions of $\mathcal{T}$ and $\mathcal{S}$, we find the following two conditions:

$$\delta D(1-\alpha) = \alpha(1-\alpha), \tag{22}$$

$$\gamma(1-\gamma) = (1-\beta)(1-\gamma). \tag{23}$$

The first condition is common with models IA and IB; the second one appears exclusively here. The latter one, unlike models IA and IB, fixes β, i.e., relates it with γ. Thus β is no longer a free parameter. Using these conditions one can arrive at the following relations:

$$\alpha = D\delta, \quad \gamma = (1-\beta), \tag{24}$$

as found in Ref. [19]. Thus, $\delta = \alpha/D$ approaches zero in the thermodynamic limit, since D scales with N and $\alpha \sim O(1)$. In the main part of the article, we primarily concern ourselves with the nature of domain walls. Analyses of the

other phases including the phase diagrams are made available in the Appendices.

For a domain wall, we set $\alpha = \beta$. This implies $J_{\mathcal{T}} = \alpha(1-\alpha)$ in the bulk of $\mathcal{T}$. Hence Eq. (21) can be rewritten as

$$\delta = (1-\alpha)\left(1 - \frac{r\alpha}{d}\right) \to 0. \tag{25}$$

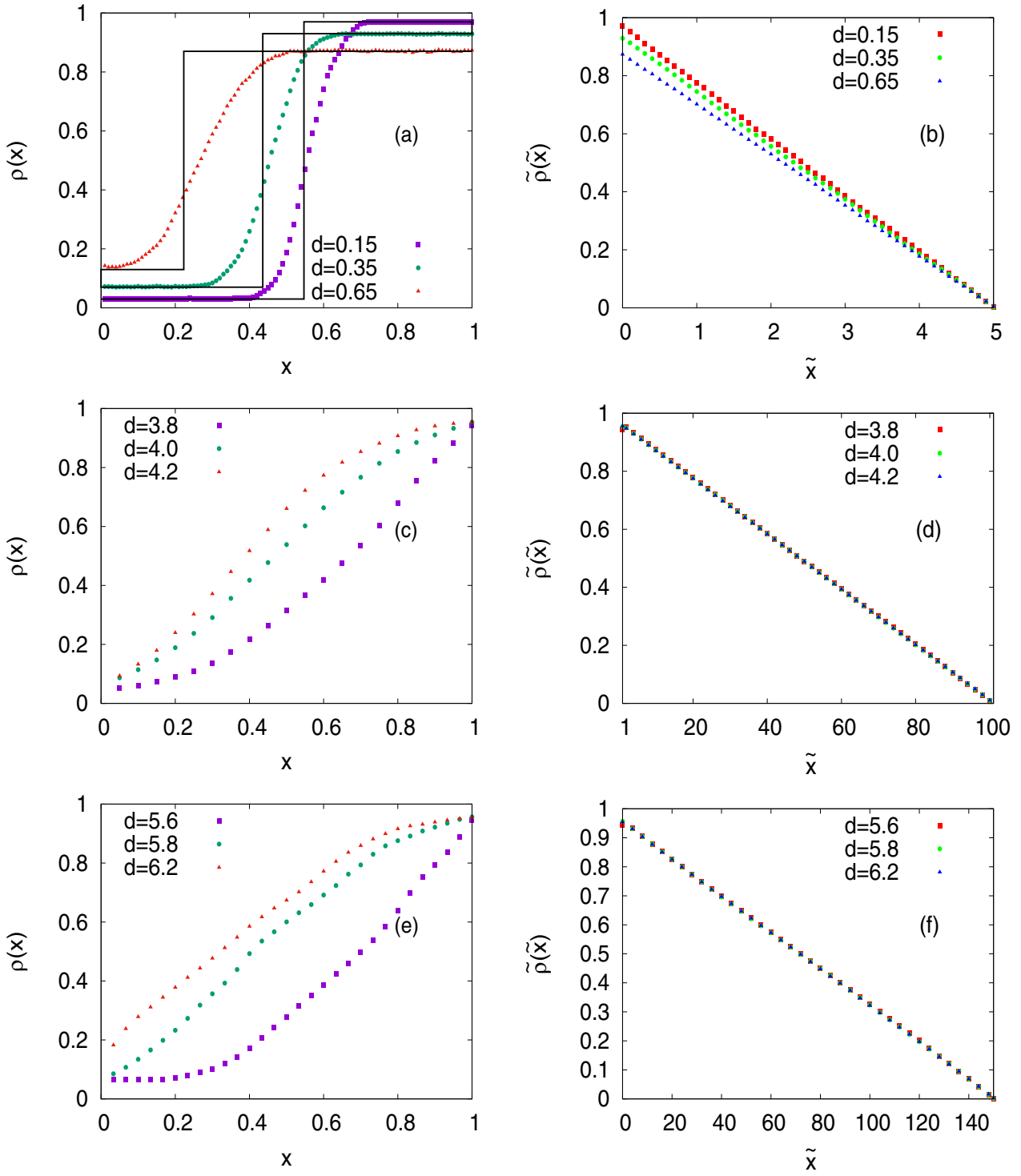

FIG. 9. Delocalization of the domain wall in $\mathcal{T}$ in model II. Steady-state plots of $\rho(x)$ versus x (left panel figures) and $\tilde{\rho}(\tilde{x})$ versus $\tilde{x}$ (right panel figures) for $N = 100$, $r = 5$ [(a) and (b)]; for $N = 100$, $r = 100$ [(c) and (d)] and $N = 150$, $r = 150$ [(e) and (f)] for $n_p = 0.48$ for different values of d. Step functions in black in (a) are MFT predictions for $\rho(x)$ (LDWs); dotted lines are MCS results for $\rho(x)$ and $\tilde{\rho}(\tilde{x})$; see also Fig. 19 in Appendix C.

This then gives $\alpha = \frac{d}{r}$. For a domain wall at x_w in $\mathcal{T}$, $\rho(x)$ is given by Eq. (5); the steady density in $\mathcal{S}$ is still given by Eq. (3). Now from particle number conservation,

$$n_p(1+r) = \int_0^{x_w} \alpha\, dx + \int_{x_w}^{1} (1-\beta) dx + \int_0^{r} [\delta + (\gamma - \delta)\tilde{x}/r] d\tilde{x}. \tag{26}$$

Solving these in the thermodynamic limit the DW position is given by (see Appendix C)

$$x_w = \frac{2n_p r(1+r) - (r-d)(2+r)}{4d - 2r}. \tag{27}$$

MF solution (27) yields the *mean position* x_w of the domain wall that is parametrized by d, r, n_p. This matches with the result in Ref. [19] for $r = 1$, for which an LDW is obtained, as expected. Surprisingly, for $r \gg 1$ the nature of the domain wall changes drastically, as found in the MCS studies (see Fig. 9 below). Our MF analysis has been complemented by MCS. We have plotted $\rho(x)$ for $N = 100$, $r = 5$, and $n_p = 0.48$ for different diffusion coefficient d in Fig. 9 (top). It is evident from the plot that for small $r(=5)$, the domain wall is pinned, i.e., an LDW is observed. We have also plotted the $\rho(x)$ for $N = 100, 150$ with $r = N$ for $n_p = 0.48$ for different d in Fig. 9 (middle and bottom, respectively). For large values of r, the LDW is found to take the shape of a DDW in an open TASEP. We also notice no significant change in the shape of the LDW as N rises keeping $r = N$.

Thus, we notice that as r rises for a fixed d and n_p, the domain wall gradually delocalizes and we eventually obtain an LDW that resembles a *single DDW* for $r \gg 1$. For $r = 1$, we reproduce the results of Ref. [19]. With a rising r, the particle content in $\mathcal{S}$ increases. We thus find that as the particle content in $\mathcal{S}$ rises (with a corresponding rise in r), the LDW in $\mathcal{T}$ gradually takes the shape of a DDW, a feature common with models IA and IB.

The explanation for the crossover from an LDW to a single DDW-like domain wall in model II as r rises to a large value runs exactly parallel to the analysis in Sec. III A 3. As in models IA and IB, the existence of a domain wall that spans the whole of $\mathcal{T}$ implies that the particle number fluctuations in $\mathcal{T}$ should scale with N. Conservation of the total particle number implies equal and opposite particle number fluctuations to take place in $\mathcal{S}$. Indeed, we find in our MCS studies that $\Delta_{\mathcal{S}}$ and $\Delta_{\mathcal{T}}$ are equal (see Fig. 10 for a plot of Δ_S versus Δ_T in model II).

As for model IA or model IB, in analogy with an ideal gas or a collection of noninteracting particles, variance Δ_s in the total number of particles in $\mathcal{S}$ should be $O(rN)$: $\sqrt{\Delta_s} \sim \sqrt{rN}$. Clearly, in the limit $r \sim O(1)$, $\sqrt{\Delta_s} \ll O(N)$, fluctuations in x_w are negligible; hence an LDW is observed. In contrast for $r \simeq N$, $\sqrt{\Delta_s} \sim O(N)$, i.e., the fluctuations in x_w are large; hence the LDW visually resembles a DDW in an open TASEP. This can be shown more formally for $\overline{N}_s/(rN) \ll 1$ for which exclusion is unimportant. In that limit the probability that two particles can occupy the same site is very small. Now define a random variable $m_{\tilde{i}}$ for every site $\tilde{i}$ of $\mathcal{S}$ that takes the value 1 if occupied with probability p, or 0 if unoccupied with probability $(1-p)$.

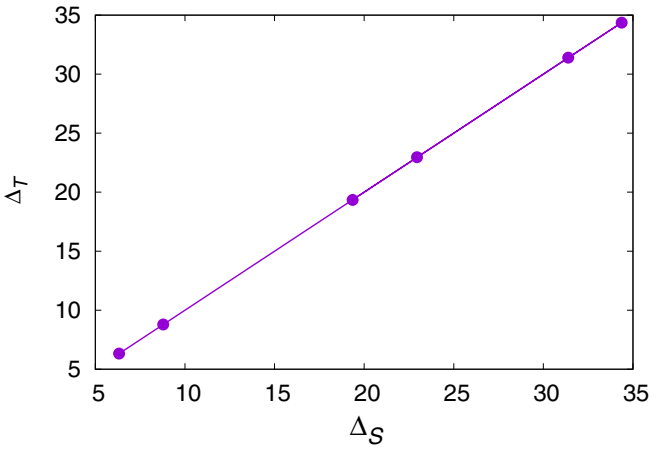

FIG. 10. Plot of Δ_S versus Δ_T in model II.

Further assume that $m_{\tilde{i}}$ are uncorrelated for different $\tilde{i}$. Therefore,

$$\langle m_{\tilde{i}} \rangle = p = \langle m_{\tilde{i}}^2 \rangle. \tag{28}$$

This gives

$$N_s = \sum_{\tilde{i}} m_{\tilde{i}}. \tag{29}$$

This implies

$$\Delta_s = \langle N_s^2 \rangle - \langle N_s \rangle^2 = \left\langle \left(\sum_{\tilde{i}} m_{\tilde{i}} \right)^2 \right\rangle - \left\langle \sum_{\tilde{i}} m_{\tilde{i}} \right\rangle^2 = \sum_{\tilde{i}} \langle m_{\tilde{i}}^2 \rangle - \sum_{\tilde{i}} \langle m_{\tilde{i}} \rangle^2 = rNp(1-p), \tag{30}$$

for small $\overline{N}_s$. When $\overline{N}_s/(rN)$ is not very small, there will be corrections to it; we ignore that issue. For an LDW that resembles a DDW in an open TASEP in model II, $\sqrt{\Delta_s} \sim \sqrt{\overline{N}_s} \sim \sqrt{rN} \sim O(N)$. This gives

$$r \sim N \tag{31}$$

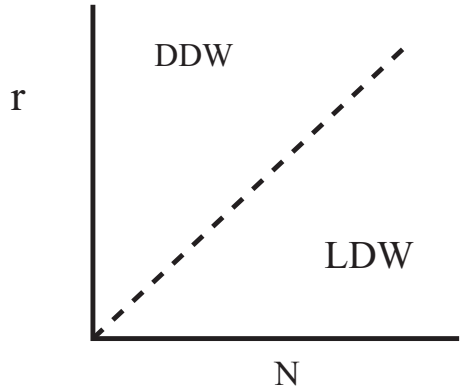

FIG. 11. A schematic state diagram for model II in the N-r plane when the conditions of a domain wall are fulfilled. The broken demarcation line is not a sharp boundary (see text).

as the threshold for a DDW in model II, which, however, is not a sharp boundary (see Fig. 11 for a schematic state diagram in the N-r plane, when the conditions of a domain wall are fulfilled). In the studies of Ref. [19], $r = 1$, giving $\Delta_T \sim O(1)$. Thus the relative fluctuation $\sqrt{\Delta_T}/N \to 0$ in the thermodynamic limit, in agreement with an LDW obtained there.

IV. CONCLUSIONS

We have studied the steady states in periodic heterogeneous exclusion processes which are composed of one TASEP ($\mathcal{T}$) and one diffusive ($\mathcal{S}$) segment. We mainly focus on the nature of the domain wall in the system. We argue that a sufficiently large particle content in $\mathcal{S}$ can delocalize the LDW to a DDW-like domain wall. In order to establish the robustness of this delocalization, we have constructed three different models depending on the choices for the dynamics in $\mathcal{S}$. MCS studies of all these models reveal a generic depinning of an LDW yielding a single DDW for sufficiently large $\overline{N}_s$, the average total particle number in $\mathcal{S}$ in the steady states. We then argue that this depinning may be explained in terms of the particle number fluctuations in $\mathcal{S}$ that increases monotonically with r and also with particle density n_p. This mechanism should be generic; a pinned shock in any closed heterogeneous TASEP is expected to get depinned by this mechanism. For instance, in the well-known models for TASEPs with finite resources [26], where reservoirs do not have any internal dynamics of their own, a single LDW in the TASEP is expected to get delocalized by the mechanism illustrated here. For a DDW in an open TASEP, MFT does not yield any mean position, which is related to the lack of any particle number conservation and the associated random particle entry or exit events. In contrast, in the present study, particle number conservation strictly holds even for large n_p and/or large r; as a result MFT, which is argued to be exact in these systems, does predict a mean position of the LDW; however, it assumes the form of a DDW by virtue of the large fluctuations of the particle content in $\mathcal{T}$ for large n_p and/or large r. Nonetheless, from an experimental point of view, there is no real distinction between a DDW in an open TASEP, and a DDW-like domain wall in the present model.

We expect our studies to be potentially relevant to protein synthesis in a cell. In live eukaryotic cells, the supply of ribosomes (modeled by particles in TASEP) is finite. For low resources, a conventional LDW may be observed, whereas for larger resources, an LDW that resembles a DDW in an open TASEP may be found. Since such an LDW necessarily implies larger fluctuations, it can be experimentally detected in standard ribosome density mapping experiments [27]. The Nagel-Schreckenberg (NaSch) model was originally introduced as a paradigmatic model for highway traffic [28]. Fluctuations in the NaSch model are shown to belong to the 1D KPZ universality class [29]. It would be interesting to extend our study to the NaSch model and study the behavior of shocks and their possible delocalization in this model and in related complex networks. In addition, the results obtained here may be verified in model experiments on the collective motion of driven particles with light-induced activity [30] in a closed narrow circular channel [16,31] with a segment enforcing directional motion, and the remaining part allowing diffusive motion within it. The ensuing steady-state densities can be measured by microscopy with image processing. While this experiment might be technically challenging, we hope this will be realized in near future. Our results on large fluctuations in closed TASEPs should make potential connections with the recently developed fluctuation theorems for nonequilibrium systems and their applications in biologically relevant systems [32]. We hope our studies will provide further impetus to future studies along these directions.

ACKNOWLEDGMENTS

A.B. thanks the Alexander von Humboldt Stiftung, Germany for partial financial support through the Research Group Linkage Programme (2016). A.K.C. gratefully acknowledges the financial support from the Science and Engineering Research Board (SERB), DST, Government of India (Project File No. ECR/2016/000848).

APPENDIX A: DOMAIN WALLS IN MODEL IA

We now provide the detailed derivation for the domain-wall position x_w in model IA. Since multiple occupancy in the diffusive channel is allowed, γ, δ are unrestricted and can assume any value. Using (4) for $J_{\mathcal{S}}$ and equality of $J_{\mathcal{S}}$ and $J_{\mathcal{T}}$ at the two junctions of $\mathcal{S}$ and $\mathcal{T}$ implies

$$\alpha(1-\alpha) = (\gamma - \delta)D/Nr, \quad D\delta(1-\alpha) = \alpha(1-\alpha). \tag{A1}$$

Hence $\delta = \frac{\alpha}{D} \sim O(1)$. Since particles from $\mathcal{T}$ are free to exit at a rate β independent of γ at the first site of $\mathcal{S}$, there is no connection between γ and β. Using $\delta = \frac{\alpha}{D}$ we have from Eq. (A1),

$$\gamma = \left[\alpha(1-\alpha) + \frac{\alpha}{Nr}\right]\frac{Nr}{D}. \tag{A2}$$

From particle number conservation one can write for the total particle number N_p,

$$N_p = \int_0^1 \rho(x) N\, dx + \int_0^r \tilde{\rho}(\tilde{x}) N\, d\tilde{x}. \tag{A3}$$

Let x_w be the position of the DW. Then density distribution in the TASEP channel $\rho(x) = \alpha + \Theta(x - x_w)(1 - \alpha - \beta)$ and that in the diffusive channel $\tilde{\rho}(\tilde{x}) = \delta + (\gamma - \delta)\tilde{x}/r$. For a domain wall to exist $\alpha = \beta$. These allow us to write

$$\begin{aligned} n_p(1+r) &= \int_0^{x_w} \alpha\, dx + \int_{x_w}^1 (1-\alpha) dx \\ &\quad + \int_0^r [\delta + (\gamma - \delta)\tilde{x}/r] d\tilde{x} \\ &= x_w(2\alpha - 1) + (1-\alpha) + r\delta/2 + r\gamma/2 \\ &= x_w(2\alpha - 1) + (1-\alpha) \\ &\quad + \frac{Nr^2}{2D}\left[\alpha(1-\alpha) + \frac{\alpha}{Nr}\right] + \frac{r\alpha}{2D}. \end{aligned} \tag{A4}$$

Hence,

$$x_w = \frac{n_p(1+r) - (1-\alpha) - \frac{Nr^2}{2D}[\alpha(1-\alpha)] - \frac{r\alpha}{D}}{(2\alpha - 1)} \quad \text{(A5)}$$

gives the position of the domain wall in MFT. The density profiles for the different phases from the MCS studies of Model IA, IB and II have been shown in Figs. 12, 13 and 14, respectively. The kymograph which represents DDW in Model IA has been shown in Fig. 15.

Phase diagram of model IA

As mentioned earlier, the phase space of model IA is spanned by three parameters:- n_p, D, and β. As explained above, for $\beta < 1/2$, LD and HD are the only possible phases, with the possibilities of an LD-HD coexistence phase in the form of a domain wall. The phase boundaries between the LD, LD-HD, and HD phases may be obtained as follows.

The boundary between the LD and the LD-HD coexistence regions may be obtained by setting $x_w = 1$ in Eq. (A5). This gives

$$D = \frac{Nr^2\beta(1-\beta) + 2r\beta}{2[n_p(1+r) - \beta]}. \quad \text{(A6)}$$

Similarly, the phase boundary between the HD and LD-HD phases is obtained by setting $x_w = 0$ in Eq. (A5), giving

$$D = \frac{Nr^2\beta(1-\beta) + 2r\beta}{2[n_p(1+r) - (1-\beta)]}. \quad \text{(A7)}$$

For $\beta > 1/2$, it has been argued that only LD and MC phases are possible with no HD phase. The phase boundary between the LD and MC phases in the n_p-D plane for a given β may be obtained as follows.

In the LD phase bulk density in $\mathcal{T}$ is $\rho(x) = \alpha$ and in the MC phase $\rho(x) = 1/2$. In $\mathcal{S}$ is $\tilde{\rho}(\tilde{x}) = \delta + (\gamma - \delta)\frac{\tilde{x}}{r}$. From particle number conservation

$$n_p(1+r) = \alpha \int_0^1 dx + \int_0^r [\delta + (\gamma - \delta)\tilde{x}/r] d\tilde{x}. \quad \text{(A8)}$$

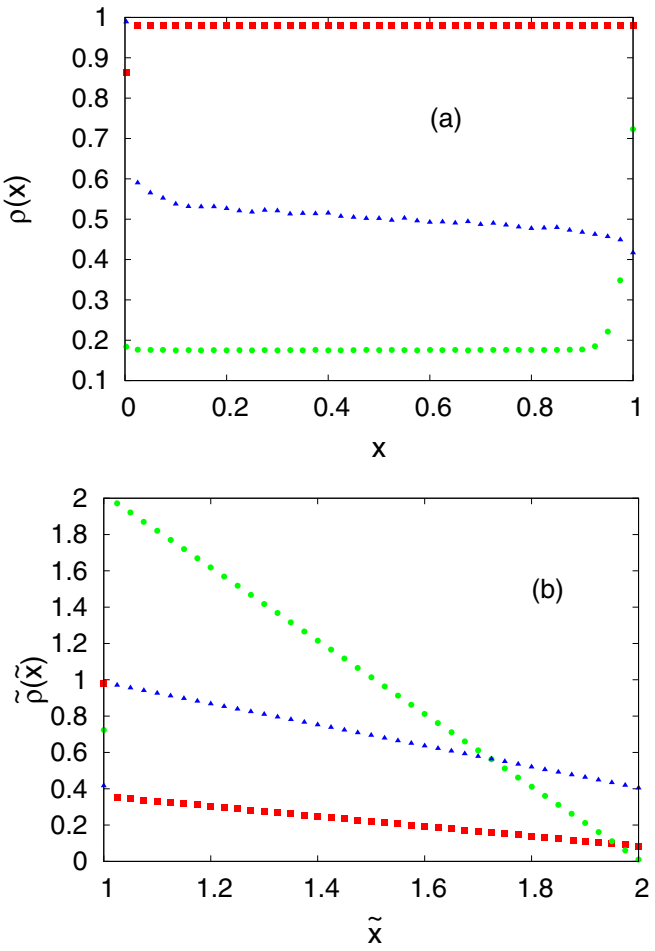

FIG. 12. Plots of (a) $\rho(x)$ versus x, and (b) $\tilde{\rho}(\tilde{x})$ versus $\tilde{x}$ in model IA from MCS studies for $N = 400$, $r = 1$ for HD (red square), LD (green circle), and MC (blue triangle) phases. HD phase corresponds to $D = 28.8$, $n_p = 0.6$, $\beta = 0.02$; LD phase corresponds to $D = 28.8$, $n_p = 0.6$, $\beta = 0.2$; and MC phase corresponds to $D = 172.8$, $n_p = 0.6$, $\beta = 0.6$.

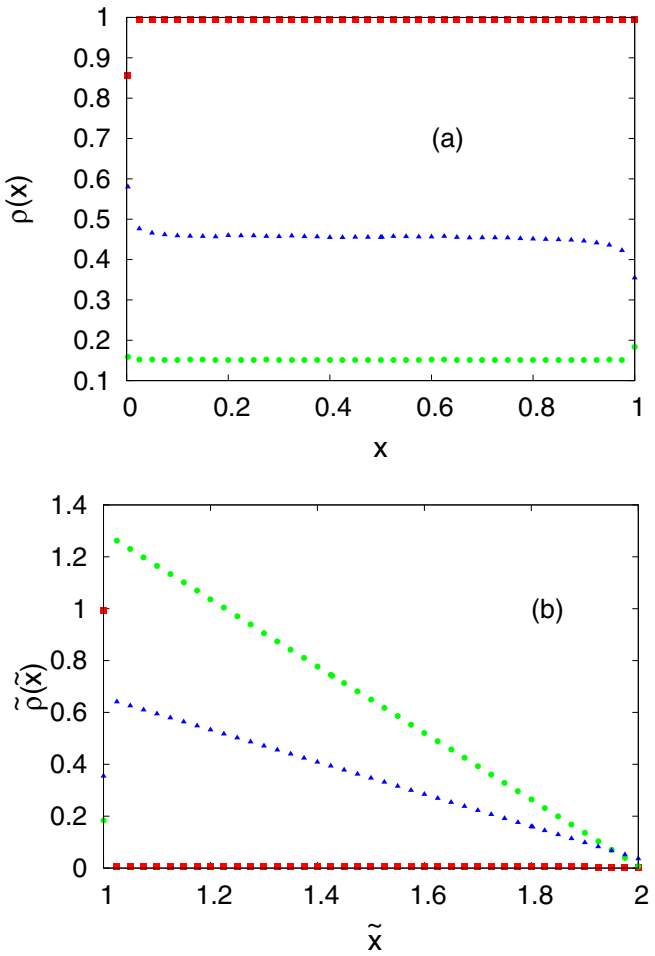

FIG. 13. Plots of (a) $\rho(x)$ versus x, and (b) $\tilde{\rho}(\tilde{x})$ versus $\tilde{x}$ in model IB from MCS studies for $N = 400$, $r = 1$ for HD (red square), LD (green circle), and MC (blue triangle) phases. HD phase corresponds to $d = 1.6$, $n_p = 0.5$, $\beta = 0.005$; LD phase corresponds to $d = 0.1$, $n_p = 0.4$, $\beta = 0.7$, and MC phase corresponds to $d = 0.4$, $n_p = 0.4$, $\beta = 0.7$.

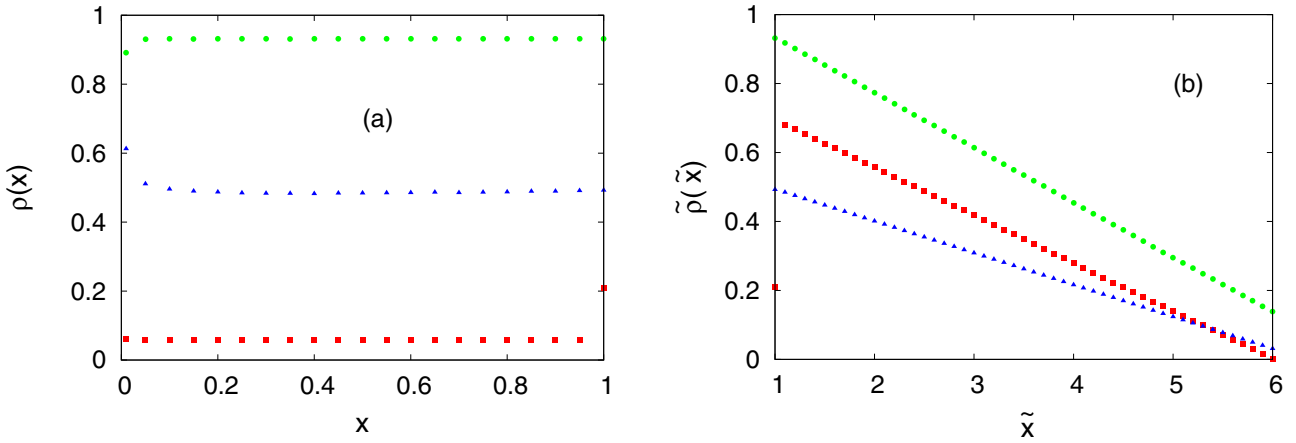

FIG. 14. Plots of (a) $\rho(x)$ versus x, and (b) $\tilde{\rho}(\tilde{x})$ versus $\tilde{x}$ from MCS studies in model II for $N = 100$, $r = 5$ for HD (green circle), LD (red square), and MC (blue triangle) phases. HD phase corresponds to $d = 0.4$, $n_p = 0.6$; LD phase corresponds to $d = 0.4$, $n_p = 0.3$; and MC phase corresponds to $d = 2.7$, $n_p = 0.3$.

Current continuity at junction B gives $\delta D(1-\alpha) = \alpha(1-\alpha)$. Using this condition one can write $\delta = \frac{\alpha}{D}$. The equality of $J_{\mathcal{T}}$ and $J_{\mathcal{S}}$ in the steady states implies $\alpha(1-\alpha) = (\gamma - \delta)D/Nr$. Hence, $\gamma = \alpha(1-\alpha)\frac{Nr}{D} + \frac{\alpha}{D}$. Using these equations for γ and δ one can obtain from Eq. (A8)

$$n_p(1+r) = \alpha + \alpha\frac{r}{D} + \frac{\alpha(1-\alpha)}{D}\frac{Nr^2}{2}. \tag{A9}$$

For $\beta > 1/2$, as long as $\alpha < 1/2$ we satisfy the condition for the LD phase. As α exceeds $\frac{1}{2}$, we satisfy the condition for the MC phase. Thus the phase boundary in the n_p-D plane between the LD and MC phases is obtained by substituting $\alpha = \frac{1}{2}$ in Eq. (A9) as

$$n_p(1+r) = \frac{1}{2} + \frac{r}{2D} + \frac{r^2N}{8D}. \tag{A10}$$

For $\beta = 1/2$, when $\alpha < 1/2$ the LD phase ensues with a bulk density $\rho(x) = \alpha$, whereas for $\alpha > 1/2$ in a given region of the phase space in the n_p-D plane, the bulk density in $\mathcal{T}$ is $\rho = 1/2$ with a *boundary layer* at $x = 0$. This is reminiscent of the density profile in an open TASEP at the boundary of the MC and HD phases. See phase diagrams in Fig. 16; our MFT and MCS results agree well.

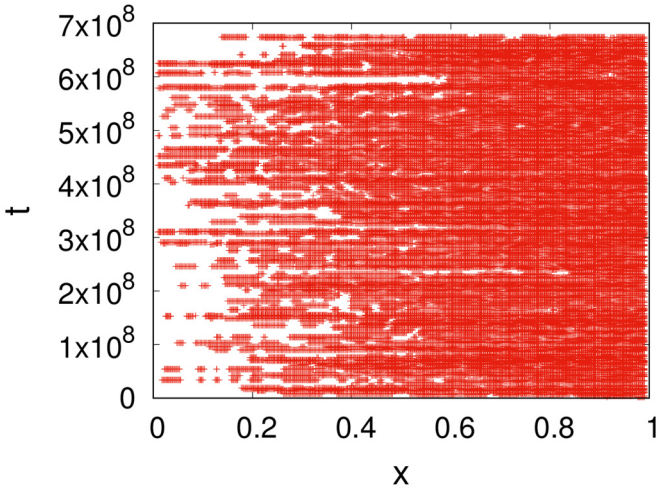

FIG. 15. Kymograph for $\rho(x)$ in model IA for $N = 400$, $r = 2$, $d = 0.715$, $\beta = 0.0052$, and $n_p = 20.0$. This strongly resembles a DDW (see Fig. 4).

APPENDIX B: DOMAIN WALLS IN MODEL IB

The detailed derivation for the position of the DW x_w in model IB is given below. When D scales with system size N we set $D = dN$ with $d \sim O(1)$. Current continuity at junction A gives $\delta D(1-\alpha) = \alpha(1-\alpha)$. Using this condition one can write $\delta = \frac{\alpha}{D} \sim O(1/N)$. Here $\delta \to 0$ in the thermodynamic limit, which is different from model IA.

We focus on the formation of the DW for which $\alpha = \beta$. The equality of $J_{\mathcal{T}}$ and $J_{\mathcal{S}}$ in the steady states implies

$$\alpha(1-\alpha) = (\gamma - \delta)D/Nr. \tag{B1}$$

Using $\delta \to 0$ in the thermodynamic limit we have from Eq. (B1),

$$\gamma = \frac{Nr}{D}[\alpha(1-\alpha)]. \tag{B2}$$

For a DW to exist, one must have $\alpha = \beta < 1/2$.

From particle number conservation one can write

$$N_p = \int_0^1 \rho(x)N\,dx + \int_0^r \tilde{\rho}(\tilde{x})N\,d\tilde{x}. \tag{B3}$$

Let x_w be the position of the DW. Now as in model IA, we have

$$\begin{aligned} n_p(1+r) &= \int_0^{x_w} \alpha\,dx + \int_{x_w}^1 (1-\alpha)dx \\ &\quad + \int_0^r [\delta + (\gamma-\delta)\tilde{x}/r]d\tilde{x} \\ &= x_w(2\alpha - 1) + (1-\alpha) + r\delta/2 + r\gamma/2. \end{aligned} \tag{B4}$$

Here in the thermodynamic limit, $\delta \to 0$. Using the expression of γ from Eq. (B2) the location x_w of the domain wall is given by

$$x_w = \frac{n_p(1+r) - (1-\alpha) - \frac{r^2}{2d}[\alpha(1-\alpha)]}{(2\alpha - 1)}. \tag{B5}$$

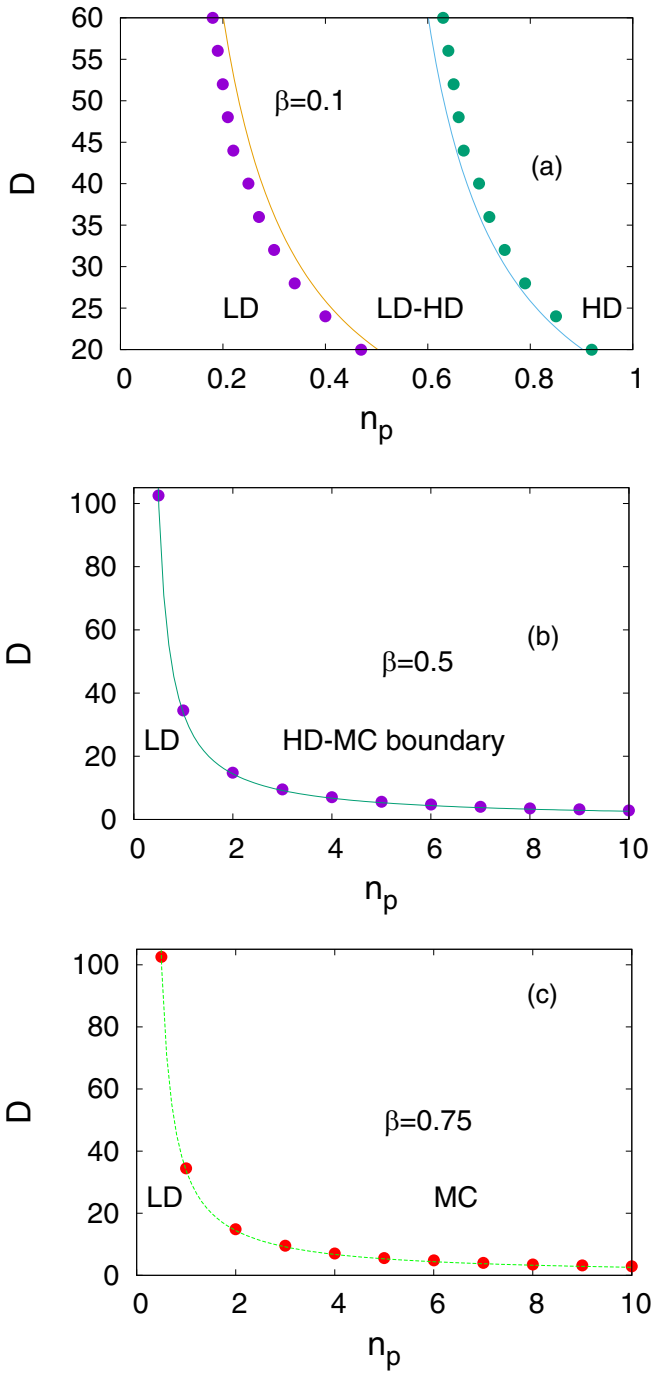

FIG. 16. Phase diagrams for model IA for three different values of β: (a) $\beta = 0.1$, (b) $\beta = 0.5$, and (c) $\beta = 0.75$. In each of the figures, a solid line represents MFT results and circles MCS data.

The kymograph obtained for Model IB has been shown in Fig. 17.

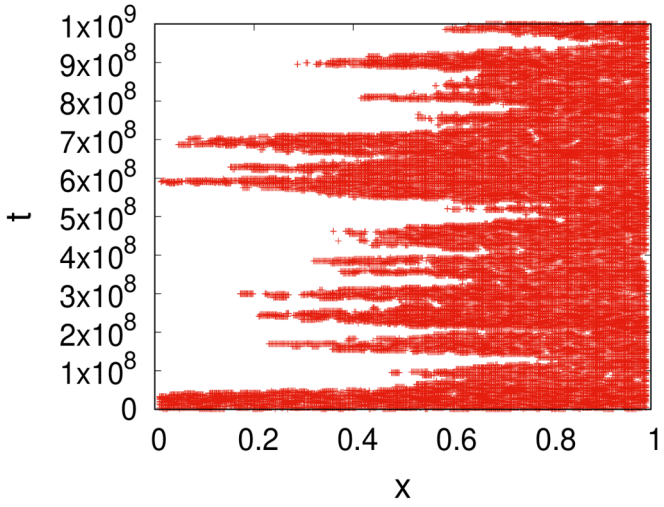

FIG. 17. Kymograph for $\rho(x)$ in model IB for $N = 400$, $r = 2$, $d = 0.006\,32$, $\beta = 0.1$, and $n_p = 10.0$, obtained from MCS studies. This is consistent with the DDWs in $\mathcal{T}$ (see Fig. 6).

Phase diagram of model IB

As mentioned earlier, the phase space of model IB is spanned by three parameters: n_p, $d = D/N$, and β. As explained above, for $\beta < 1/2$, LD and HD are the only possible phases, with the possibilities of an LD-HD coexistence phase in the form of a domain wall. The phase boundaries between the LD, LD-HD, and HD phases may be obtained as follows.

For $x_w \leqslant 0$ the DW leaves $\mathcal{T}$ at the left junction resulting in the HD phase having constant density $\rho(x) = 1 - \beta$, $x_w \geqslant 1$ results in the LD phase having constant density $\rho(x) = \alpha$, and the LD-HD phase is characterized by the presence of a DW inside the system for $0 < x_w < 1$.

Hence the boundary between the HD and LD-HD coexistence regions may be obtained by setting $x_w = 0$ in Eq. (B5). This gives

$$d = \frac{r^2\beta(1-\beta)}{2[n_p(1+r) - (1-\beta)]}. \tag{B6}$$

Similarly the boundary between the LD and LD-HD coexistence regions is obtained by setting $x_w = 1$ in Eq. (B5) which gives

$$d = \frac{r^2\beta(1-\beta)}{2[n_p(1+r) - \beta]}. \tag{B7}$$

For $\beta > 1/2$, only the LD and MC phases are possible with no HD phase. The phase boundary between the LD and MC phases in the n_p-d plane for a given β may be obtained as follows.

In the LD phase bulk density in $\mathcal{T}$ is $\rho(x) = \alpha$ and in the MC phase $\rho(x) = 1/2$. In $\mathcal{S}$ is $\tilde{\rho}(\tilde{x}) = \delta + (\gamma - \delta)\frac{\tilde{x}}{r}$. From particle number conservation (PNC)

$$n_p(1+r) = \alpha \int_0^1 dx + \int_0^r [\delta + (\gamma - \delta)\tilde{x}/r] d\tilde{x}. \tag{B8}$$

Using the expressions of γ and δ for model IB in Eq. (B8) we obtain

$$n_p(1+r) = \alpha + \frac{\alpha(1-\alpha)}{D}\frac{Nr^2}{2}. \tag{B9}$$

For $\beta > 1/2$, as long as $\alpha < 1/2$ we satisfy the condition for the LD phase. As α exceeds $\frac{1}{2}$, we satisfy the condition for the MC phase. Thus the phase boundary in the n_p-D plane between the LD and MC phases is obtained by substituting

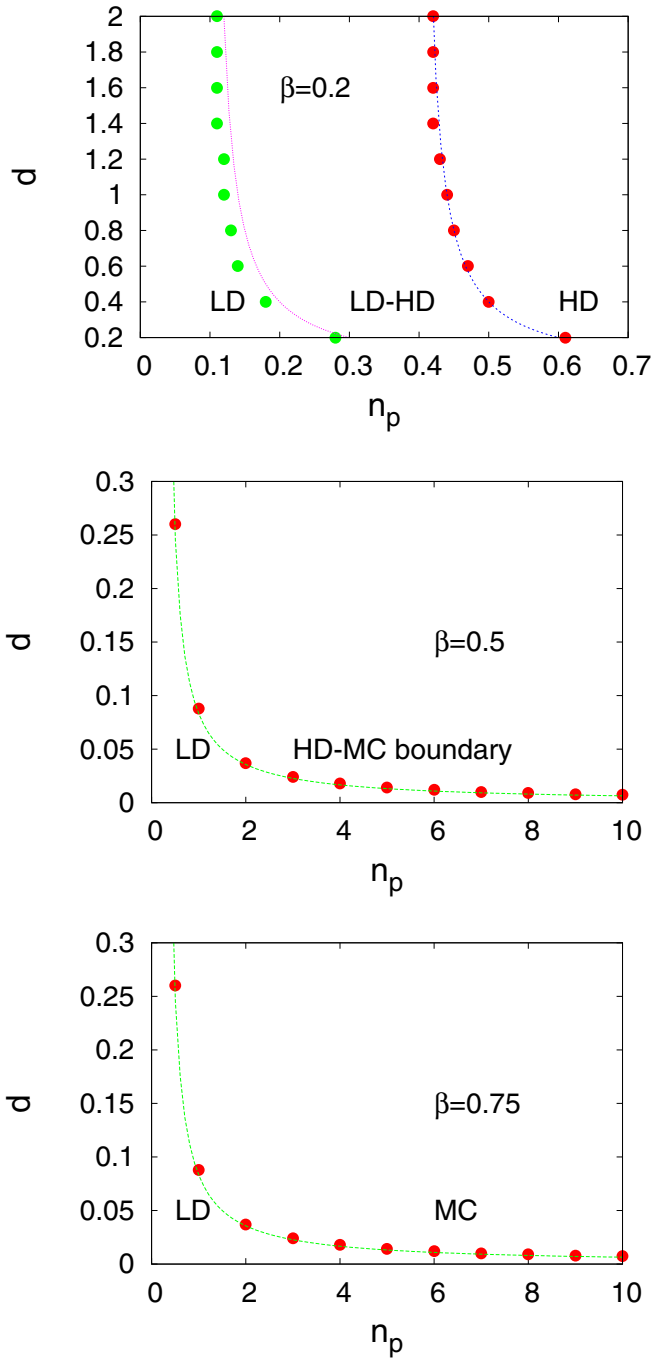

FIG. 18. Phase diagrams for model IB for three different values of β: (a) $\beta = 0.2$, (b) $\beta = 0.5$, and (c) $\beta = 0.75$. In each of the figures, a solid line represents the MFT results and circles the MCS data.

$\alpha = \frac{1}{2}$ in Eq. (B9) as

$$n_p(1+r) = \frac{1}{2} + \frac{r^2 N}{8D}. \tag{B10}$$

For $\beta = 1/2$, when $\alpha < 1/2$ the LD phase ensues with a bulk density $\rho(x) = \alpha$, whereas for $\alpha > 1/2$ in a given region of the phase space in the n_p-D plane, the bulk density in $\mathcal{T}$ is $\rho = 1/2$ with a *boundary layer* at $x = 0$. This is reminiscent of the density profile in an open TASEP at the boundary of the

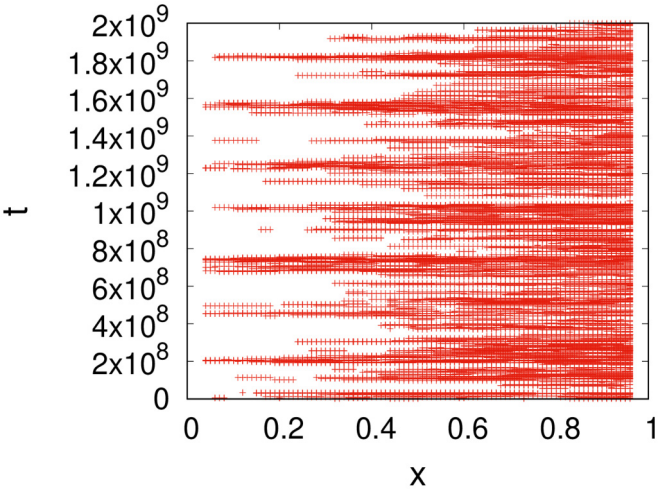

FIG. 19. Kymograph for $\rho(x)$ in model II for $N = 100$ with $r = 100$, $d = 4.0$, and $n_p = 0.48$. This corresponds to a DDW-like domain wall in Fig. 9(e).

MC and HD phases. See phase diagrams in Fig. 18; our MFT and MCS results are close to each other.

APPENDIX C: DOMAIN WALLS IN MODEL II

From particle number conservation one can write

$$N_p = \int_0^1 \rho(x) N\, dx + \int_0^r \tilde{\rho}(\tilde{x}) N\, d\tilde{x}. \tag{C1}$$

Density distribution in the TASEP channel $\rho(x) = \alpha + \Theta(x - x_w)(1 - \alpha - \beta)$ and that in the diffusive channel $\tilde{\rho}(\tilde{x}) = \delta + (\gamma - \delta)\tilde{x}/r$. This implies

$$\begin{aligned} n_p(1+r) &= \int_0^{x_w} \alpha\, dx + \int_{x_w}^1 (1-\beta) dx \\ &\quad + \int_0^r [\delta + (\gamma - \delta)\tilde{x}/r] d\tilde{x} \\ &= \alpha x_w + (1-\beta)(1-x_w) + \frac{r\gamma}{2}. \end{aligned} \tag{C2}$$

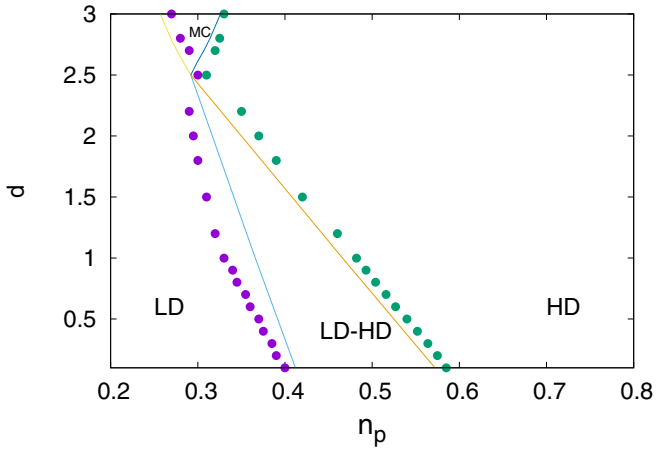

FIG. 20. Solid lines represent the phase diagram obtained using MFT and the circles represent the same obtained using MCS for model II for $r = 5$. The phase diagram exhibits four different phases.

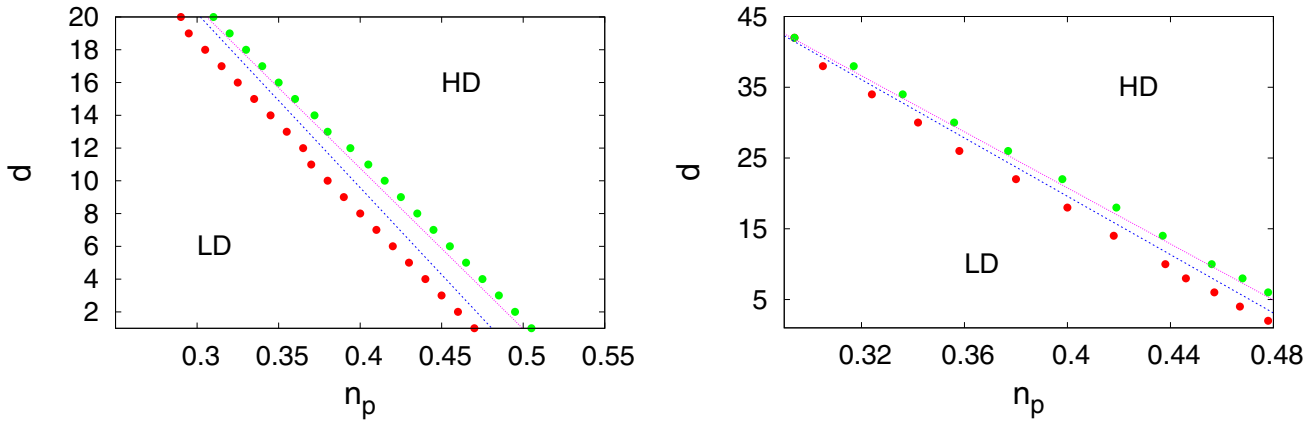

FIG. 21. Phase diagram of model II: (a) $r = 50$ and (b) $r = 100$. Solid lines represent the phase boundaries obtained from MFT and the circles represent the same obtained using MCS.

Since $\delta \sim O(1/N)$ in the thermodynamic limit, $\delta \to 0$ and $\alpha \to \frac{d}{r}$. Also from Eq. (24) $\gamma = 1 - \beta$. Now from the condition of DW $\alpha = \beta$. Using these conditions we have from Eq. (C2),

$$x_w = \frac{2r(1+r)n_p - (r-d)(2+r)}{4d - 2r}. \tag{C3}$$

The kymograph obtained for Model II has been shown in Fig. 19.

Phase diagrams for model II

For different values of r we can get a phase diagram in (n_p, d) space consisting of different regimes depending on the position of the DW. For $x_w \leqslant 0$ the DW leaves the active part at the left junction resulting in the HD phase having constant density $\rho(x) = 1 - \beta$; $x_w \geqslant 1$ results in the LD phase having constant density $\rho(x) = \alpha$ and the LD-HD phase is characterized by a DW localized inside the system for $0 < x_w < 1$. From Eq. (C3) the phase boundary between the HD phase and the LD-HD coexistence region is given by

$$d = r - \frac{n_p 2r(1+r)}{2+r}. \tag{C4}$$

The phase boundary between the LD and LD-HD (domain wall) phases is obtained as

$$d = \frac{2n_p r(1+r) - r^2}{2-r}. \tag{C5}$$

Similar to an ordinary TASEP, the ring system also exhibits an MC phase which is characterized by maximum active part current $J_{\rm MC} = 1/4$ and constant density $\rho = 1/2$ and is obtained for $\alpha, \beta > 1/2$. Hence, $N/2$ particles have to be present in the active part. Equality of the active part current and passive part current allows one to write $\gamma = \delta + \frac{r}{4d}$.

Particle number conservation in the MC phase gives

$$(1+r)n_p = r\left(\delta + \frac{r}{8d}\right) + \frac{1}{2}. \tag{C6}$$

The constraints $\alpha, \beta > 1/2$ on the active part impose constraints on the passive part by the use of Eqs. (21) and (24) as

$$\delta > \frac{1}{2dN} \tag{C7}$$

and

$$\delta < \frac{1}{2} - \frac{r}{4d}. \tag{C8}$$

Implementing Eq. (C7) in Eq. (C6) one can get a phase boundary between the LD and MC phases in the thermodynamic limit as

$$d = \frac{r^2}{8(1+r)n_p - 4}. \tag{C9}$$

Similarly the phase boundary between the HD and MC phases can be obtained using Eq. (C8) in Eq. (C6) as

$$d = \frac{r^2}{4(1+r)(1-2n_p)}. \tag{C10}$$

The phase diagrams in the (n_p-d) plane for model II are shown in Figs. 20 and 21 for different values of r.

[1] P. M. Chaikin and T. C. Lubensky, *Principles of Condensed Matter Physics* (Cambridge University Press, Cambridge, UK, 2000).

[2] A. L. Barabasi and H. E. Stanley, *Fractal Concepts in Surface Growth* (Cambridge University Press, Cambridge, 1995).

[3] J. T. MacDonald, J. H. Gibbs, and A. C. Pipkin, Biopolymers **6**, 1 (1968).

[4] J. Krug, Phys. Rev. Lett. **67**, 1882 (1991).

[5] B. Derrida, E. Domany, and D. Mukamel, J. Stat. Phys. **69**, 667 (1992); G. Schütz and E. Domany, *ibid.* **72**, 277 (1993); B. Derrida, M. R. Evans, V. Hakim, and V. Pasquier, J. Phys. A: Math. Gen. **26**, 1493 (1993); G. Schütz, J. Stat. Phys. **88**, 427 (1997).

[6] R. A. Blythe and M. R. Evans, J. Phys. A: Math. Theor. **40**, R333 (2007).

[7] T. Chou, K. Mallick, and R. K. P. Zia, Rep. Prog. Phys. **74**, 116601 (2011).
[8] A. B. Kolomeisky, J. Phys.: Condens. Matter **25**, 463101 (2013).
[9] P. C. Bressloff and J. M. Newby, Rev. Mod. Phys. **85**, 135 (2013).
[10] C. Appert-Rolland, M. Ebbinghaus, and L. Santen, Phys. Rep. **593**, 1 (2015).
[11] S. Katz, J. L. Lebowitz, and H. Spohn, J. Stat. Phys. **34**, 497 (1984).
[12] D. Chowdhury, L. Santen, and A. Schadschneider, Phys. Rep. **329**, 199 (2000).
[13] D. Lips, A. Ryabov, and P. Maass, Phys. Rev. Lett. **121**, 160601 (2018).
[14] Q. Y. Hao, R. Jiang, C. Y. Wu, N. Guo, B. B. Liu, and Y. Zhang, Phys. Rev. E **98**, 062111 (2018).
[15] R. Lipowsky, S. Klumpp, and T. M. Nieuwenhuizen, Phys. Rev. Lett. **87**, 108101 (2001).
[16] S. Bleil, 1 P. Reimann, and C. Bechinger, Phys. Rev. E **75**, 031117 (2007).
[17] N. Sarkar and A. Basu, Phys. Rev. E **90**, 022109 (2014).
[18] S. A. Janowsky and J. L. Lebowitz, Phys. Rev. A **45**, 618 (1992).
[19] H. Hinsch and E. Frey, Phys. Rev. Lett. **97**, 095701 (2006).
[20] T. Banerjee, N. Sarkar, and A. Basu, J. Stat. Mech. (2015) P01024.
[21] R. Jiang, Y. Q. Wang, A. B. Kolomeisky, W. Huang, M. B. Hu, and Q. S. Wu, Phys. Rev. E **87**, 012107 (2013).
[22] Y.-Q. Wang, R. Jiang, Q.-S. Wu, and H.-Y. Wu, Mod. Phys. Lett. B **28**, 1450064 (2014).
[23] Y.-Q. Wang, R. Jiang, A. B. Kolomeisky, and M. B. Hu, Sci. Rep. **4**, 5459 (2014).
[24] I. Neri, N. Kern, and A. Parmeggiani, Phys. Rev. Lett. **110**, 098102 (2013); Q.-S. Wu, Mod. Phys. Lett. B **28**, 1540064 (2014); see also [23] for other recent extensions of the model in Ref. [19].
[25] The two choices of $D \sim O(1)$ and $D \sim O(N)$ are just two possible choices (among many others) that allow for finite steady-state currents. These two choices suffice for our purposes here.
[26] L. J. Cook and R. K. P. Zia, J. Stat. Mech. (2009) P02012.
[27] See, e.g., N. Eldad and Y. Arava, in *Post-Transcriptional Gene Regulation*, edited by J. Wilusz (Humana Press, Totowa, NJ., 2008).
[28] K. Nagel and M. Schreckenberg, J. Phys. I **2**, 2221 (1992).
[29] J. de Gier, A. Schadschneider, J. Schmidt, and Gunter M. Schütz, Phys. Rev. E **100**, 052111 (2019).
[30] I. Buttinoni, G. Volpe, F. Kümmel, G. Volpe, and C. Bechinger, J. Phys.: Condens. Matter **24**, 284129 (2012).
[31] C. Bechinger, R. DiLeonardo, H. Lowen, C. Reichhardt, G. Volpe, and G. Volpe, Rev. Mod. Phys. **88**, 045006 (2016).
[32] U. Seifert, Rep. Prog. Phys. **75**, 126001 (2012).